

Magnetoresistance oscillations arising from edge-localized electrons in low-defect graphene antidot-lattices

T. Shimizu, J. Nakamura, K. Tada, Y. Yagi, and J. Haruyama

Citation: *Appl. Phys. Lett.* **100**, 023104 (2012); doi: 10.1063/1.3675547

View online: <http://dx.doi.org/10.1063/1.3675547>

View Table of Contents: <http://apl.aip.org/resource/1/APPLAB/v100/i2>

Published by the [American Institute of Physics](#).

Related Articles

Correlation between the ferromagnetic metal percolation and the sign evolution of angular dependent magnetoresistance in Pr_{0.7}Ca_{0.3}MnO₃ film

Appl. Phys. Lett. **99**, 252502 (2011)

Charge carrier mobility and concentration as a function of composition in AgPO₃-AgI glasses

J. Chem. Phys. **135**, 234504 (2011)

Weak localization and antilocalization of hole carriers in degenerate p-Ge_{1-x}Mn_xTe

J. Appl. Phys. **110**, 113916 (2011)

Enhanced low-field magnetoresistance in La_{0.67}Sr_{0.33}MnO₃:MgO composite films

J. Appl. Phys. **110**, 113913 (2011)

Tuning magnetoresistance and exchange coupling in ZnO by doping transition metals

Appl. Phys. Lett. **99**, 222503 (2011)

Additional information on *Appl. Phys. Lett.*

Journal Homepage: <http://apl.aip.org/>

Journal Information: http://apl.aip.org/about/about_the_journal

Top downloads: http://apl.aip.org/features/most_downloaded

Information for Authors: <http://apl.aip.org/authors>

ADVERTISEMENT

**AIP**Advances

Submit Now

**Explore AIP's new
open-access journal**

- **Article-level metrics
now available**
- **Join the conversation!
Rate & comment on articles**

Magnetoresistance oscillations arising from edge-localized electrons in low-defect graphene antidot-lattices

T. Shimizu, J. Nakamura, K. Tada, Y. Yagi, and J. Haruyama^{a)}

Faculty of Science and Engineering, Aoyama Gakuin University, 5-10-1 Fuchinobe, Sagamihara, Kanagawa 252-5258, Japan

(Received 31 July 2011; accepted 12 December 2011; published online 9 January 2012)

The so-called zigzag edge of graphenes has localized and strongly spin-polarized electrons. However, magnetoresistance (MR) behavior associated with the edge electrons has not been reported in graphenes. Here, we measure MR of graphene antidot-lattices, honeycomb-like arrays of hexagonal antidots with a large ensemble of hydrogen-terminated and low-defect antidot edges, prepared by a nonlithographic method using nanoporous alumina templates. We find anomalous MR oscillations arising from localized electron spins existing at the antidot edges. These are promising for realization of spintronic devices. © 2012 American Institute of Physics. [doi:10.1063/1.3675547]

The zigzag-atomic structure of the edge of graphene (Fig. 1(a)) theoretically has a high electronic density of states (EDOS; edge states) owing to its strongly localized electrons, which originate from the presence of flat energy bands near the Fermi level (E_F).^{1,2} The localized edge electron spins are stabilized and strongly polarized depending on the exchange interaction between the two edges, leading to maximum spin ordering in these orbitals, similar to the case of Hund's rule for atoms. Theoretical studies include those on graphene nanoribbon (GNR; an one-dimensional (1D) restriction of graphene with edges on both longitudinal sides),^{3,4} and on graphene with (hexagonal) antidot (ADs; i.e., nanopores) lattices (Fig. 1(a)).^{5-7,16-20} These highly localized electrons can introduce (anti)ferromagnetism in GNRs.^{1,2} Previously, we have reported ferromagnetism arising from AD-edge-localized electron spins in low-defect graphene AD lattices (GADLs) with honeycomb-like arrays of hexagonal ADs.⁵

On the other hand, the formation of AD lattices (ADLs) on compound semiconductor two-dimensional electron gas (2DEG) systems has been shown to introduce various quantum phenomena under a magnetic field (B) (see supplementary material (6) (Ref. 21)).⁸⁻¹² Electrons adopt cyclotron motion under B applied perpendicular to the 2DEG. This led to rich physics (quantum phenomena), depending on the relationship between the aspect ratio (AD diameter ϕ to the period a of the ADL: Fig. 2(a)) and the classical radius of the cyclotron orbit, $R_c = (\pi n_S)^{1/2} (h/2\pi)/eB$, where n_S is the charge density and h and e are Planck's constant and the electron charge, respectively. For instance, commensurability magnetoresistance (MR) peaks and Aharonov-Bohm (AB)-type oscillations¹² (with an oscillation period $\Delta B_{ABT} = (h/e)S$, where S is the area of the unit cell; Fig. 2(a)) were observed around B at where electrons encircle and localize around the ADs (i.e., at $2R_c = a$). In the present GADL, $R_c = 75$ nm at $B = 1.2$ T is estimated from Fig. 2(b)) for large ϕ/a with narrow inter-AD spacing (see supplementary material (6)).²¹ In contrast, when the ADL acts as a scattering center for cyclo-

tron electrons in small- ϕ/a samples, anomalous fractional quantum Hall effect (QHE) was observed.⁹

In GADLs, electrons can localize at the zigzag-AD edges even without B , as mentioned above.⁵ Nevertheless, the correlation between electron localization and MR

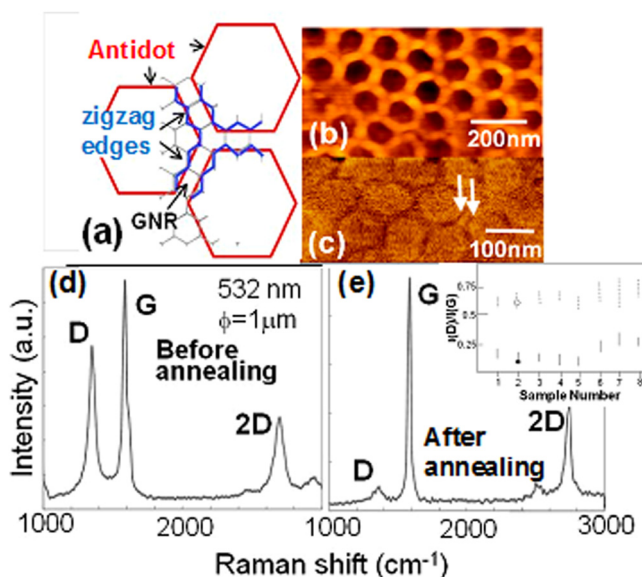


FIG. 1. (Color online) (a) Schematic view of a honeycomb-like GADL, which shows the situation where the boundaries are aligned with the carbon hexagonal lattice of graphene to form a zigzag edge. Narrow spaces between two ADs correspond to GNRs with width W . The actual structure has a larger number of hexagonal carbon unit cells per GNR (length ~ 40 nm and $W \sim 20$ nm). This GADL provides at least three large advantages (see supplementary material (2)).²¹ (b) AFM image of GADL formed using an etching mask with mean AD diameter $\phi \sim 80$ nm and $W \sim 20$ nm. (c) MFM image of an H-terminated GADL. A CoPtCr-coated Si probe was used for measurements in tapping mode. The inter-AD regions, which exhibit darker color, imply a high density of polarized spins. In particular, evidence for AD-edge-localized spins may be seen in the parts shown by the arrows. (d)(e) Typical Raman spectra of a GADL (d) prior and (e) after annealing at 800°C , taken with a laser excitation of 532 nm and 0.14 mW incident power at room temperature. Because the laser beam diameter ϕ used for the measurement is 1 μm , the result reflects edge information from ~ 60 ADs. Inset of (e) distribution of $I(D)/I(G)$ in 8 samples. 15 points at 5 different positions were observed per sample. Dotted and solid lines above and below 0.5 denote $I(D)/I(G)$ prior and after annealing, respectively. Black and open symbols correspond to the main panels of (d) and (e), respectively.

^{a)} Author to whom correspondence should be addressed. Electronic mail: J-haru@ee.aoyama.ac.jp.

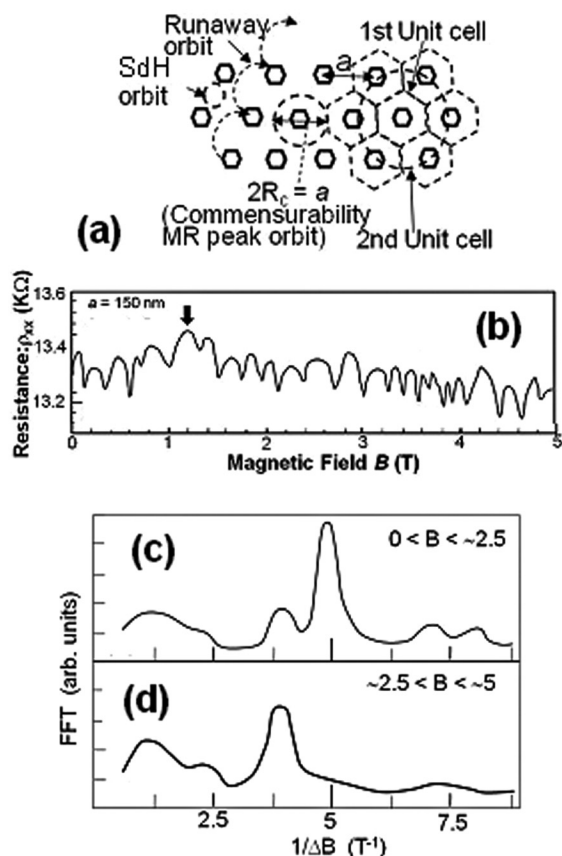


FIG. 2. (a) Schematic views of electron trajectories under magnetic fields and the unit cells in a honeycomb-like GADL (see supplementary material (6)). (b) MR (ρ_{xx}) measurements of the hydrogen-terminated ~ 10 -layer GADL (with a mean $\phi \sim 80$ nm and mean $a \sim 150$ nm, implying an aspect ratio $\phi/a \sim 0.5$) as a function of B applied perpendicular to the GADL at $T = 1.5$ K. Measurements were performed by a standard low-frequency (13 Hz) ac lock-in technique using a constant excitation current of 1 nA. (c) (d) Fourier power spectra of sample in (b) for (c) low B and (d) high B regions.

behavior has not been explored, although some experiments without considering edge effects reported MR behavior in GADLs.^{16,17} Thus, it is crucial to reveal how the AD-edge-localized electrons interact with the cyclotron-motion electrons under B and produce novel quantum MR behavior.

In the present study, low-defect GADLs with honeycomb-like arrays of hexagonal ADs (Fig. 1(a)) are fabricated on a large ensemble of mechanically exfoliated graphenes by a non-lithographic method using a nanoporous alumina template (NPAT) (Ref. 13) (see supplementary material (1) and (2) (Ref. 21)).⁵ Using the NPAT as a mask, assembled graphenes were etched under carefully optimized conditions using low-power Ar gas to avoid damaging the AD edges (see supplementary material (3) and (4)).²¹ The boundaries of ADs are not intentionally aligned along the hexagonal carbon lattice of graphene in this process.

All GADLs fabricated through these processes were annealed at 800°C in high vacuum (10^{-6} Torr) for 0.5–3 days and then in hydrogen gas for 1–3 h prior to measurements.⁵ These annealing processes cause possible reconstruction of edge atomic structures to zigzag with ferromagnetism as mentioned later.

Figure 1(a) shows a schematic view of GADL with zigzag AD edges. Atomic force microscopy (AFM) images of GADL formed as described above are presented in Fig. 1(b),

which shows the hexagonal shape of the AD. A magnetic force microscope (MFM) image is shown in Fig. 1(c). The inter-AD (GNR) regions exhibit a uniform darker color which is clear evidence for a high density of polarized spins in agreement with the theoretical results for zigzag-GNRs mentioned above.⁵

Figures 1(d) and 1(e) show typical Raman spectra of a GADL before and after annealing. The intensity of the D peak, $I(D)$, is significantly reduced after annealing and, thus, the $I(D)/I(G)$ value drastically decreases from 0.6 to 0.8 to less than ~ 0.5 upon annealing (inset of Fig. 1(e)). In particular, samples 1–4 exhibit very low $I(D)/I(G)$, below 0.2. The low $I(D)/I(G)$ values conventionally suggest high-quality carbon crystals with a low volume of defects (disorder, impurities). We have previously demonstrated³ that defects and disorder in GNRs could be drastically reduced by annealing at 800°C .

More importantly, the low $I(D)/I(G)$ value implies not only a reduction of defects but also an enhanced alignment of pore boundaries to give pure zigzag edges via reconstruction during high-temperature annealing (see supplementary material (12),²¹ Refs. 5, 6 and 14), although we did not intentionally align the pore edges to produce pure zigzag structure unlike Ref. 6 (see supplementary material (5)).²¹

It has, however, been suggested that after Joule heating, a mixture of zigzag and armchair edges in graphitic nanoribbons reconstructs towards mostly zigzag edges.¹⁵ In our system, we argue that the annealing at a temperature of 800°C for narrow (~ 20 nm) GNRs can play a similar role to that of Joule heating, because GADLs typically disappear upon annealing at $T > 800^\circ\text{C}$. Moreover, Ref. 5 showed that GADLs with similar characteristics to those in Fig. 1 and low $I(D)/I(G)$ values, as shown in the inset of Fig. 1(e), exhibited ferromagnetism. Therefore, these strongly support the presence of zigzag AD edges with localized and spin-polarized electrons in the present GADLs. This is also consistent with the MFM observation (Fig. 1(c)).

To reveal the correlation between the AD-edge-localized electrons and MR behavior, Figure 2(b) shows the result of an MR (ρ_{xx}) measurement of the H-terminated ~ 10 -layer ADLGs (see supplementary material (7)).²¹ A broad MR peak is visible at $B \sim 1.2$ T (arrows in Fig. 2(b)). The change in the MR value is only slight relative to the peak value as B increases, owing to the residual 3D nature of the ~ 10 -layer GADL (see supplementary material (8)).²¹ Thereafter, periodic MR oscillations are observed over a wide range of B spanning up to 5 T, although they become ambiguous at some B values.

Such MR peak and periodic MR oscillations have been observed in 2DEGs (Refs. 8–12), as mentioned above. Electron trajectories that encircle the ADs cause electrons to localize around the ADs (Fig. 2(a)), resulting in a MR peak (i.e., commensurability peak of MR) and in subsequent AB-type oscillations (see supplementary material (9)).²¹ The latter effect requires the mean free path to be as small as the order of a ($a \sim 150$ nm for the present GADLs) to allow the formation of quantized electron orbitals around the AD edges. In the present GADLs, $\phi/a \sim 0.5$ lies within the crossover region between the regimes of small and large ϕ/a . Thus, the MR peak observed at $B \sim 1.2$ T in Fig. 2(b) corresponds to the commensurability MR peak. From $2R_c = 2(\pi n_S)^{1/2} (h/2\pi)/$

$eB = a$, we estimate $n_S \sim 4 \times 10^{11} \text{ cm}^{-2}$ and an elastic mean free path $l_e = 2D/v_F$ (where D is the diffusion constant and v_F is the Fermi velocity) $\sim 800 \text{ nm}$, in approximate agreement with Ref. 8. Therefore, the present GADL can demonstrate AB-type oscillations, because the length of the circumference of the first unit cell shown in Fig. 2(a) is $2\pi(a/2) \sim 540 \text{ nm} < l_e \sim 800 \text{ nm}$. To determine the exact oscillation periods in Fig. 2(b), Fourier transformation was performed. Figures 2(c) and 2(d) show the Fourier power spectra calculated over the ranges $0 < B < 2.5 \text{ T}$ and $2.5 < B < 5 \text{ T}$, respectively, for the sample shown in Fig. 2(b). We find two-different peaks in the low and high B regions.

At low B (Fig. 2(c)), a sharp peak appears around $1/\Delta B \sim 5 \text{ T}^{-1}$. The corresponding oscillation period $\Delta B \sim 200 \text{ mT}$ is consistent with that expected of AB-type oscillations, where the magnetic flux enclosed within the first unit cell of the honeycomb (hexagonal) ADL (i.e., Wigner-Seitz cell in Fig. 2(a)) changes by a single flux quantum for each period, i.e., $\Delta B_{ABT} = (h/e)/S$ with $a \sim 160 \text{ nm}$, where $S = 6(3^{-1/2}/2)(a/2)^2$. On the other hand, at high B (Fig. 2(d)), this peak disappears. This is because R_c decreases as B increases and cyclotron orbits strongly localize at the AD edges above B values for which $2R_c < \phi$ or $(a-\phi)$.^{8,9} Because the critical B value for disappearance of the AB-type effect is $\sim 2.4 \text{ T}$ in the present system, the disappearance of the $1/\Delta B \sim 5 \text{ T}^{-1}$ peak in Fig. 2(d) is relevant.

In turn, another large peak at $1/\Delta B \sim 3.8 \text{ T}^{-1}$ becomes considerable in Fig. 2(d). The corresponding oscillation period is $\Delta B \sim 260 \text{ mT}$, which is larger than $\Delta B \sim 200 \text{ mT}$ for the low B region. We reveal that this smaller oscillation period originates from R_c , which is smaller than the radii associated with the AB-type effect and exactly corresponds to the radius ($\phi/2$) of the ADs. This is unique to the present GADLs and emphasizes the strong contribution of the edge-localized electrons within a few nanometers of the AD edge, which were confirmed in Fig. 1(c) and Ref. 5.

Two interpretations are possible for this original peak at high B : (1) AB effect with $\Delta B_{AB} = (h/e)/(\pi r^2)$ (Ref. 16) and (2) quantization of the single particle spectrum according to the Bohr–Sommerfeld quantization condition with $\Phi = B\pi r^2 = m(h/e)$, where Φ and m are the magnetic flux and an integer. For case (1), $\Delta B \sim 260 \text{ mT} = (h/e)/(\pi r^2)$ gives $r \sim 40 \text{ nm}$. This r value is close to $\phi/2 \sim 45 \text{ nm}$ in the present AD and suggests that the edge-localized electrons combined with cyclotron electrons can form an AB-ring current. However, the AB effect should not theoretically appear in the ADL system, because it is smoothed by statistical averaging over a large ensemble of ADs (see supplementary material (9)).²¹

For case (2), $\Phi = B\pi r^2 = m(h/e)$ corresponds to quantization of magnetic flux, Φ , as for flux quanta in superconductors. As for case (1), $\Delta B \sim 260 \text{ mT} = (h/e)/(\pi r^2)$ gives $r \sim 40 \text{ nm}$, which is close to $\phi/2 \sim 45 \text{ nm}$. This suggests that the edge-localized electrons combined with cyclotron electrons can quantize Φ penetrating into an AD. Each when one flux quantum penetrates into the AD, one MR oscillation is added. In the case of a type-II superconductor system, Meissner loop current yields flux quantum to conserve its phase and subsequent superconductivity. The edge-localized current here can cause similar behavior to keep the current itself, avoiding its disappearance by phase interference.

In any case, the peak observation at high B (Fig. 2(d)) suggests the cause from strongly localized currents at the AD-edges. This is unique to the present GADLs, because the electron current cannot exist just at the AD edges in conventional ADL systems such as semiconductor 2DEG, for some reason (e.g., electron depletion regions from etching damage). Thus, this suggests an advantage of the present low-defect GADLs fabricated by nonlithographic method combined with low-power Ar etching (see supplementary material (2)).²¹ Moreover, a possible AB-type effect has even been detected for the larger (2nd) unit cell (see supplementary material (11)).²¹

It is expected that QHEs will ideally be observed in high-mobility monolayer GADLs with a small ϕ/a fabricated following the present nonlithographic method, in conjunction with the MR features discussed here (see supplementary material (13)).²¹ Electron correlations in such a system would undoubtedly produce interesting quantum phenomena (e.g., an anomalous fractional QHE).^{11,12} We also envisage the application of GADLs to arrays of GNRs for the purpose of fabricating semiconducting operation devices.^{7,18,20}

The authors thank K. Fujita, Y. Hashimoto, E. Endo, Y. Iye, S. Katsumoto, M. Yamamoto, S. Tarucha, T. Ando, K. Wakabayashi, T. Enoki, N. Nagaosa, T. Yamaoka, P. Kim, X. Jia, and M. S. Dresselhaus for their technical contribution, fruitful discussions, and encouragement. This work was partly supported by a Grant-in-aid for Scientific Research and a High-Technology Research Center Project for private universities from MEXT, Kyoto University Zero-Emission Energy Project, and AOARD funding.

¹K. Nakada, M. Fujita, G. Dresselhaus, and M. S. Dresselhaus, *Phys. Rev. B* **54**, 17954 (1996).

²M. Fujita, K. Wakabayashi, K. Nakata, and K. Kusakabe, *J. Phys. Soc. Jpn.* **65**, 1920 (1996).

³T. Shimizu, J. Haruyama, D. C. Marcano, D. V. Kosinkin, J. M. Tour, K. Hirose, and K. Suenaga, *Nat. Nanotechnol.* **6**, 45 (2011).

⁴M. Y. Han, J. C. Brant, and P. Kim, *Phys. Rev. Lett.* **104**, 056801 (2010).

⁵K. Tada, J. Haruyama, H. X. Yang, M. Chshiev, T. Matsui, and H. Fukuyama, *Appl. Phys. Lett.* **99**, 183111 (2011); *Phys. Rev. Lett.* **107**, 217203 (2011).

⁶B. Krauss, P. N. Incze, V. Skakalova, L. P. Biro, K. von Klitzing, and J. J. Smet, *Nano Lett.* **10**, 4544 (2010).

⁷J. Bai, X. Zhong, S. Jiang, Y. Huang, and X. Duan, *Nat. Nanotechnol.* **5**, 190 (2010).

⁸D. Weiss, K. Richter, A. Menschig, R. Bergman, H. Schweizer, K. von Klitzing, and G. Weimann, *Phys. Rev. Lett.* **70**, 4118 (1993).

⁹D. Weiss, M. L. Roukes, A. Menschig, P. Grambow, K. von Klitzing, and G. Weimann, *Phys. Rev. Lett.* **66**, 2790 (1991).

¹⁰M. Kato, A. Endo, S. Katsumoto, and Y. Iye, *Phys. Rev. B* **77**, 155318 (2008).

¹¹W. Kang, H. L. Stormer, L. N. Pfeiffer, K. W. Baldwin, and K. W. West, *Phys. Rev. Lett.* **71**, 3850 (1993).

¹²T. Ando, Y. Arakawa, K. Furuya, S. Komiyama, and H. Nakashima, *Mesoscopic Physics and Electronics* (Springer, Berlin, 1998); T. Ando, S. Uryu, and S. Ishizaka, *Jpn. J. Appl. Phys. Part 1* **38**, 308 (1999).

¹³I. Takesue, J. Haruyama, N. Kobayashi, S. Chiashi, S. Maruyama, T. Sugai, and H. Shinohara, *Phys. Rev. Lett.* **96**, 057001 (2006).

¹⁴Y. You, Z. Ni, T. Yu, and Z. Shen, *Appl. Phys. Lett.* **93**, 163112 (2008).

¹⁵X. Jia, M. Hofmann, V. Meunier, B. G. Sumpter, J. C. Delgado, J. M. R. Herrera, H. Son, Y.-P. Hsieh, A. Reina, J. Kong *et al.*, *Science* **323**, 1701 (2009).

¹⁶T. Shen, Y. Q. Wu, M. A. Capano, L. P. Rokhinson, L. W. Engel, and P. D. Ye, *Appl. Phys. Lett.* **93**, 122102 (2008).

¹⁷J. Eroms and D. Weiss, *New J. Phys.* **11**, 095021 (2009).

¹⁸M. Kim, N. S. Safron, E. Han, M. S. Arnold, and P. Gopalan, *Nano Lett.* **10**, 1128 (2010).

¹⁹M. Begliarkbekov, O. Sul, J. Santanello, N. Ai, X. Zhang, E.-H. Yang, and S. Strauf, *Nano Lett.* **11**, 1254 (2011).

²⁰T. G. Pedersen, C. Flindt, J. Pedersen, N. A. Mortensen, A.-P. Jauho, and K. Pedersen, *Phys. Rev. Lett.* **100**, 136804 (2008).

²¹See supplementary material at <http://dx.doi.org/10.1063/1.3675547> for (1)–(12) noted in text.